Journal of Alloys and Compounds 739 (2018) 882–891

Contents lists available at ScienceDirect

Journal of Alloys and Compounds

journal homepage: http://www.elsevier.com/locate/jalcom

A fast method to prepare Pd-Co nanostructures decorated on graphene as excellent electrocatalyst toward formic acid oxidation

Abdollatif Shafaei Douk*, Hamideh Saravani**, Meissam Noroozifar

Department of Chemistry, University of Sistan and Baluchestan, P.O. Box 98135-674, Zahedan, Iran

ARTICLE INFO

Article history:
Received 28 September 2017
Received in revised form
7 December 2017
Accepted 23 December 2017
Available online 29 December 2017

Keywords:
Fast method
Electrochemical reduction
Nanostructures
Galvanic replacement
Formic acid oxidation

ABSTRACT

The electrochemical reduction of cobalt (II) formate on graphene/glassy carbon electrode (G/GCE) surface in HCl (5 wt%) is used to prepare Pd-Co electrocatalyst. The Pd-Co nanostructures decorated on the graphene nanosheets were prepared in two steps: (1) electrochemical reduction of cobalt (II) formate and (2) the galvanic replacement reaction between Co and Pd^{2+}. This approach has a number of advantages including being environmentally friendly, simple, low-price, and very fast. The morphology and bulk compositions of the samples were investigated *via* Field Emission Scanning Electron Microscopy (FESEM), X-ray diffraction (XRD) patterns, Energy Dispersive X-ray Spectroscopy (EDS). Electrochemical techniques, including Cyclic Voltammetry (CV), Chronoamperometry (CA) and Electrochemical Impedance Spectroscopy (EIS) measurements were used to analyze the electrochemical activity of the samples. The peak current density for oxidation of formic acid on Pd-Co/G electrocatalyst was very high (151.32 mA cm^{-2}). The Pd-Co/G increased the current density 7.1 times more than Pd/C. Besides, the onset oxidation potential and peak potential for Pd-Co/G electrocatalyst illustrated a negative shift in comparison to Pd/C. Chronoamperometry experiment showed that the stability of the Pd-Co/G catalyst was remarkably promoted. The Pd-Co/G electrocatalyst represents extraordinary electrocatalytic activity and durability toward formic acid oxidation.

1. Introduction

Direct Formic Acid Fuel Cells (DFAFCs) have received a great deal of attention due to their several advantages, such as low toxicity, high practical power density, low operating temperature, safe storage and transportation, etc [1–5]. Nonetheless, the commercial application of DFAFCs still faces three important obstacles: insufficient performance, inadequate stability and high-price of catalysts. Therefore, the tailored design of highly active anode catalyst for the oxidation of formic acid molecules has become an active area of research.

In recent years, Pt-based nanomaterials are often used as electrocatalysts in DFAFC [6–8]. However, major problems such as high price and serious carbon monoxide (CO) poisoning of the Pt-based electrocatalysts prevent their commercial applications [9–11]. Therefore, the search for highly active, stable, and inexpensive alternative electrocatalysts to replace Pt-based electrocatalysts is of utmost importance. Nowadays, Pd-based catalysts have emerged as a promising alternative due to their low-price, larger resistance to CO poisoning, and high electrocatalytic activity [12–15]. It has been established that, formic acid on Pt and Pd-based electrocatalysts surface undergoes oxidative decomposition according to the two mechanisms described below [8,16,17]:

$$HCOOH \rightarrow CO_2 + 2H^+ + 2e^- \text{ direct pathway (dehydrogenation)} \quad (1)$$

$$HCOOH \rightarrow CO_{ads} + H_2O \text{ indirect pathway (dehydration)} \quad (2a)$$

$$CO_{ads} + H_2O \rightarrow CO_2 + 2H^+ + 2e^- \quad (2b)$$

The oxidation of formic acid based on direct oxidation to CO_2 (Eq. (1)) as a major pathway is clearly more effective than another two-step process. Indirect pathway (Eqs. (2a) and (2b)) is accompanied by the formation of carbon monoxide (CO_{ads}) intermediate species (Eq. (2a)), which are strongly bonded on the catalyst surface and lead to the catalyst deactivation. Pd, compared to Pt, represents superior electrocatalytic activity for oxidation of formic acid, which

* Corresponding author. Tel.: +98 54 3344 6565; fax: +98 54 3344 6888.
** Corresponding author.
E-mail addresses: shafaeidouk@pgs.usb.ac.ir (A. Shafaei Douk), saravani@chem.usb.ac.ir (H. Saravani).

https://doi.org/10.1016/j.jallcom.2017.12.272
0925-8388/

is attributed to the different catalytic oxidation mechanism. In comparison to the Pt and Pt-based catalysts, oxidation of formic acid is more inclined to occur through the dehydrogenation pathway (direct pathway) on the Pd catalyst [18]. Therefore, Pd-based electrocatalysts show excellent catalytic activity and stability toward formic acid oxidation.

Preparation of highly active electrocatalysts with low noble metal loading for anode is a key index for DFAFC development. It is well-known that, the performance of electrocatalysts strongly depends on the synergistic effect (electronic effect, geometric effect, bifunctional mechanism, etc.), distribution, shape, size, etc [19,20]. Therefore, a great deal of effort has been devoted to the development of the Pd-based electrocatalysts. Up to now, various methods have been developed to prepare highly active Pd-based electrocatalysts such as alloying Pd with other metals to prepare alloy catalysts [21–23] preparation of Pd nanocrystals by controlled shapes [24–27], etc. One important route is alloying Pd with other non-noble metals. This approach could not only decrease the loading of Pd metal, but also improve the electrocatalytic performance and stability. It is well known that, the incorporation of second metals such as Au [28], Co [29], Ni [30], Ag [31], and Cu [32] to the Pd, leading to the improvement of electrocatalytic activity of Pd-based electrocatalysts. In recent years, Co has been utilized as a second metal combined with Pd and Pt for the improvement of electrocatalytic activity of the Pd and Pt catalysts. During the past decades, different methods such as impregnation synthesis method [33], simultaneous reduction reaction [34], organic colloid method [35], one-pot surfactant-free route [36], co-reduction method [37], etc, have been employed to fabricate Pd-Co binary electrocatalysts toward formic acid oxidation. In previous studies, Xing et al. [38] fabricated Pd-Co electrocatalysts through a sodium borohydride reduction method and showed superior catalytic performance toward formic acid oxidation. Arriaga et al. [39] reported that Pd-Co electrocatalysts supported on multiwalled carbon nanotubes (CNTs) were prepared through an impregnation method followed by thermal treatment and used as an anode catalyst in a microfluidic formic acid fuel cell. Xu et al. [40] prepared nanoporous Pd-Co Alloy through a one-step mild dealloying of a PdCoAl precursor alloy method and showed higher electrocatalytic activity toward formic acid oxidation.

Unfortunately, a major imperfection in the fabrication and development of Pd-based binary electrocatalysts is the use of reducing reagents (such as sodium borohydride, ethylene glycol, etc) and stabilizers (such as poly(vinyl pyrrolidone) (PVP), oleylamine, etc). The reducing reagents and stabilizers are not only high price, but also dangerous reagents with respect to both human health and the environment. Furthermore, the fabrication of Pd-based binary electrocatalysts requires a long time and high temperature.

Apart from Pd alloying with non-noble metals, the desirable selection of support materials is also an important index to decrease the Pd metal loading. The recent appearance of graphene nanosheets has opened a novel road for using two-dimensional (2D) new carbon materials as support electrocatalysts owing to their remarkable conductivity, unique graphitized basal plane structure, and inexpensive preparation [41,42].

Herein, we propose a novel approach to fabricate Pd-Co nanostructures decorated on the graphene/glassy carbon electrode (G/GCE). This approach has several advantages such as simplicity, low prices, fast, environmentally friendliness and surfactant-free method. In this research, Pd-Co nanostructures decorated on the G/GCE were prepared in a much shorter duration of time at ambient condition without the use of reducing agents and stabilizers. As shown in Fig. 1, the electrochemical reduction of cobalt (II) formate is carried out in a beaker containing zinc electrode (anode), working electrode (cathode) and HCl (5 wt%) aqueous solution in Ar atmosphere at ambient temperature. The electrochemical reduction of cobalt (II) formate in cathode leads to the preparation of a Co/G/GCE modified electrode. The Pd-Co nanostructures decorated on the G/GCE are prepared through galvanic replacement Co with Pd^{2+} ions by Co/G/GCE immersed in a 0.1 M $HClO_4$ solution containing the 2.0 mM of $PdCl_2$.

2. Experimental

2.1. Chemical reagents

Palladium (II) chloride ($PdCl_2$) and cobalt (II) nitrate hexahydrate ($Co(NO_3)_2{\cdot}6H_2O$) were purchased from Sigma-Aldrich Co. Graphite powder, sodium hydroxide, formic acid, alumina (Al_2O_3) and ethanol (purity 99%) were purchased from Merck Co.

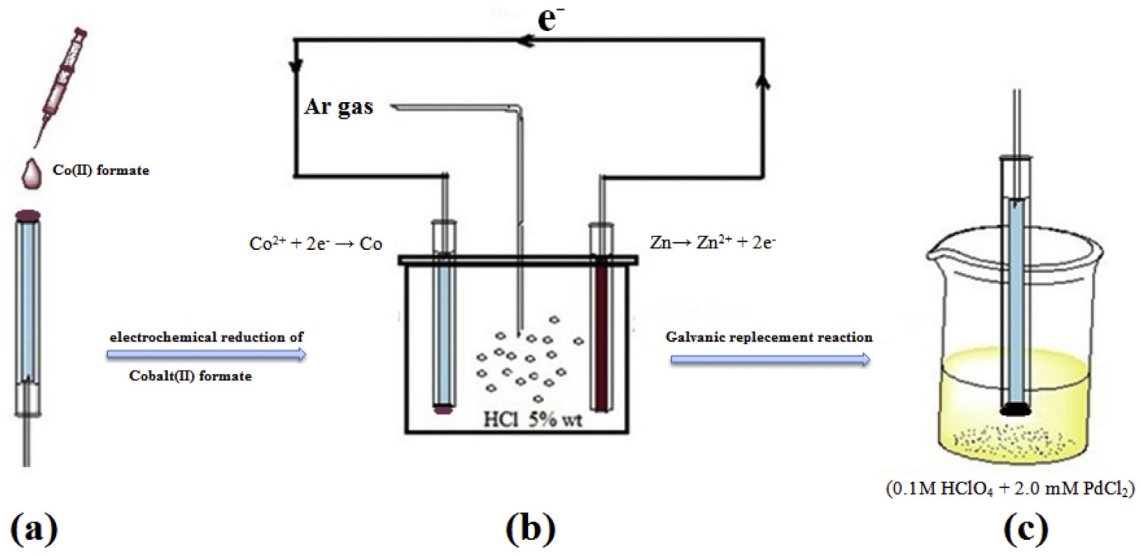

Fig. 1. Schematic the preparation of Pd-Co/G/GCE modified electrode.

2.2. Instruments

In order to study the morphology of the as-produced Pd/C and Pd-Co/G catalysts, Field Emission Scanning Electron Microscopy (FESEM) was employed. Energy-dispersive X-ray spectroscopy (EDS) was conducted to investigate the bulk composition of Pd-Co/G and Pd/C electrocatalysts. FESEM and EDS analyses were performed by using MIRA3 TESCAN and SAMX electron microscope, respectively. X-Ray Diffraction (XRD) patterns of the as-obtained Pd-Co/G and Pd/C samples were taken by a Bruker, D8 ADVANCE XRD diffraction spectrometer for 2θ values of 10–90°. XRD analyses were conducted on a Philips diffractometer of X'pert company with graphite monochromatic Cu Kα radiation source (λ = 1.54056 Å). To prepare the Pd/C catalyst ink, a 5 μL amount of the Pd/C catalyst was dispersed in the mixture of 4 ml distilled water and 1 ml chitosan (1 wt%) and sonicated for 30 min. A 5 μL portion of the resultant dispersion was transferred onto the pre-polished GCE by using a micropipette and let it dry in room condition. Electrochemical determinations were done with an SAMA-500 Electroanalyser (SAMA Research Center, Iran) controlled by a personal computer. All electrochemical examinations were recorded by using a conventional three-electrode cell system. The modified glassy carbon electrode (with 0.0314 cm^{-2} surface areas) and platinum foil served as the working electrode and the counter electrode, respectively. An Ag|AgCl electrode served as the reference electrode. Electrochemical impedance spectroscopy (EIS) was carried out with an Autolab PGSTAT 128N (EcoChemie, Netherlands) potentiostat/galvanostat controlled by NOVA 1.11 software. Electrochemical impedance measurements were performed in 5 mM $[Fe(CN)_6]^{3-/4-}$ fabricated in 0.1 M KCl. EIS was performed over a frequency region of 0.1 Hz–100 kHz with 0.02 V amplitude (rms). All electrochemical measures were recorded at room temperature (RT).

2.3. Preparation of graphene

Graphene oxide (GO) was produced with the Hummers route [43]. Next, the chemical reduction of GO to graphene was carried out [44].

2.4. Preparation of cobalt (II) formate

Cobalt (II) formate ($Co(HCOO)_2$) was prepared *via* the reaction of cobalt (II) nitrate hexahydrate ($Co(NO_3)_2 \cdot 6H_2O$) with an additional amount of sodium hydroxide (NaOH) in deionized water at ambient condition. Thereafter, the achieved precipitate was filtered and washed several times using deionized water. Then, production of cobalt (II) formate was done by adding dropwise style of formic acid into the filtered precipitate under harsh stirring until the precipitate was completely dissolved. This solution was crystallized at room condition. These cobalt (II) formate crystals were stored in a desiccator and let it dry overnight and collected for future use.

2.5. Preparation of Pd-Co nanostructures decorated on graphene

In order to prepare the Pd-Co/G/GCE modified electrode, a Glassy Carbon (GC) electrode was carefully polished with alumina powder on a polishing cloth and cleansed by sonication in absolute ethanol and deionized water and let it dry at room condition. To prepare of the working electrode, using high-power ultrasound, 5 mg of graphene was scattered in the mixture of 4 ml deionized water and 1 ml chitosan (1 wt%) solution for 30 min. A 5 μL portion of the resultant dispersion (graphene nanosheets suspension) was transferred onto the pre-polished GCE by using a micropipette and dried at ambient condition. Then 3 μL of cobalt (II) formate (1 mg/ml) solution was drop covered onto the G/GCE and let it dry in air at RT. At this point, the $Co(HCOO)_2$/G/GCE modified electrode was fabricated. The electrochemical reduction of $Co(HCOO)_2$ on the G/GCE surface was carried out in a beaker (Fig. 1(b)) having a zinc electrode as anode and $Co(HCOO)_2$/G/GCE as cathode (working electrode) in HCl (5 wt%) aqueous solution as electrolyte under an Ar gas atmosphere in two to 5 s at ambient temperature. Prior to electrochemical reduction, the electrolyte solution was de-aerated with Ar gas for 15 min. The result was a decoration of Co nanostructures on the G/GCE (working electrode) in cathode. Then, Pd nanostructures were decorated on Co/G/GCE modified electrode through the galvanic replacement between Co and Pd by immersing of a Cu/G/GCE modified electrode in the electrolyte solution containing 2.0 mM of $PdCl_2$ and 0.1 M $HClO_4$ for 300 s. For a comparison of electrocatalytic performance, a Pd/C (20 wt%) electrocatalyst was prepared according to the procedure described before [45].

3. Results and discussion

3.1. Galvanization of Pd

The Pd-Co nanostructures decorated on the graphene nanosheets were fabricated by the electrochemical reduction of cobalt (II) formate on the G/GCE surface at ambient condition followed by the galvanic replacement of Co by Pd^{2+} ions in room temperature. As shown in Fig. 1, in this approach, during the electrochemical reduction, two electrons are transferred from the zinc electrode as an anode to $Co(HCOO)_2$/G/GCE (i.e. the working electrode) as a cathode. The electron transfers between anode (zinc) and cathode (working electrode) leads to the following reactions in the anode and cathode electrode surfaces:

$$\text{Anode: } Zn \rightarrow Zn^{2+} + 2e^- \quad (3)$$

$$\text{Cathode: } Co(OOCH)_2 + 2e^- \rightarrow Co\downarrow + 2HCOO^{-1} \quad (4)$$

According to the reactions (3, 4), the electrochemical reduction reaction in the HCl (5 wt%) solution which is a spontaneous redox process, leading to the decoration of Co nanostructures on the G/GCE surface. At this point, a Co/G/GCE modified electrode is prepared. The Pd-Co nanostructures decorated on graphene nanosheets were fabricated through the galvanic replacement between Co and Pd by Co/G/GCE immersed in the electrolyte solution containing 2.0 mM of $PdCl_2$ and 0.1 M $HClO_4$ for 300 s according to reaction (5) [46].

$$Co + PdCl_2 \rightarrow Pd\downarrow + Co^{2+} + 2Cl^- \quad (5)$$

The difference in the standard redox potential of Pd and Co, leads to a galvanic replacement reaction between Pd and Co which is thermodynamically favored, as seen in eqs. (6)–(8).

$$Co \rightarrow Co^{2+} + 2e^- \; E^0 = +0.28V \quad (6)$$

$$Pd^{2+} + 2e^- \rightarrow Pd \; E^0 = +0.92V \quad (7)$$

$$Co + Pd^{2+} \rightarrow Pd + Co^{2+} \; E^0_{ov} = +1.20V \quad (8)$$

These reactions (Eqs. (6)–(8)) demonstrate the transfer of two electrons from Co to the Pd^{2+} ion. It can be seen that the value of the overall reduction redox potential is positive ($E^0 > 0$) which is favored from a thermodynamic viewpoint. The standard Gibbs free energy (ΔG^0) of the Pd-Co electrocatalyst was calculated using the following eq. (9):

$$\Delta G^0 = -nFE^0 \quad (9)$$

where, n is the number of exchanged electrons while E^0 and F are the overall standard redox potential and the Faradic constant, respectively. The positive value of the overall standard redox potential ($E^0 > 0$) and negative value of Gibbs free energy ($\Delta G^0 < 0$) demonstrate a spontaneous irreversible redox process between the Pd and Co nanostructures.

3.2. Structural characteristics

In order to study the morphology of the as-fabricated Pd-Co/G and Pd/C electrocatalysts, FESEM analysis was performed. Fig. 2 represents the FESEM images of the Pd-Co/G and Pd/C electrocatalysts. Fig. 2(a, b, c and d) exhibit the FESEM images of the electrode surface at each stage of modification. Fig. 2(a) depicts the FESEM image of the working electrode surface after covering the working electrode by graphene nanosheets. As shown, a uniform film of graphene nanosheets was covered on the GCE surface and a

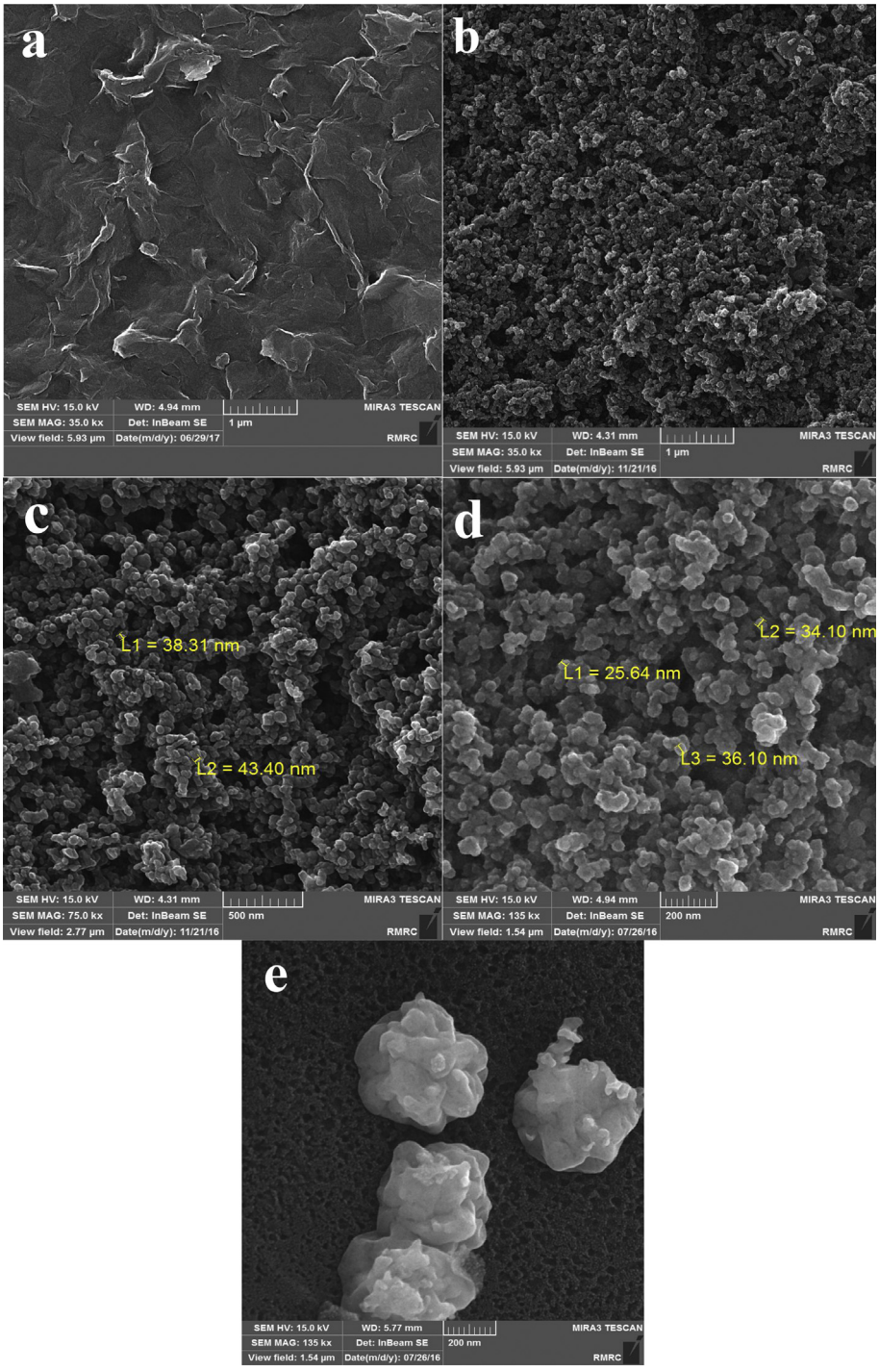

Fig. 2. The FESEM images of: G/GCE modified electrode (a), Co/G/GCE modified electrode at different magnifications (b, c), Pd-Co/G/GCE modified electrode (d) and the Pd/C (e).

G/GCE modified electrode was prepared. The FESEM images after the electrochemical reduction reaction of Co were obtained at different magnifications. Fig. 2(b) represents low magnification the FESEM image of Co nanostructures decorated on graphene nanosheets. The FESEM image after the electrochemical reduction reaction of cobalt (II) formate on the G/GCE surface and decoration of Co nanostructures on the graphene nanosheets at high magnifications is shown in Fig. 2(c). As shown in Fig. 2(b and c), the Co nanostructures were decorated uniformly on the graphene nanosheets with an average size of about 41 nm. Also, Fig. 2(d) represents the FESEM image after galvanic replacement reaction of Co by Pd and preparation of a Pd-Co/G/GCE modified electrode. The Pd-Co nanostructures were decorated on the G/GCE surface with an average size of about 32 nm. Fig. 2(e) illustrates the FESEM image of the Pd/C catalyst. This image demonstrates the accumulation of Pd nanoparticles on the carbon support.

X-ray diffraction (XRD) technique was utilized to assess the crystalline phases of the as-fabricated Pd-Co/G and Pd/C catalysts. The typical XRD patterns of the Pd-Co/G and Pd/C catalysts are presented in Fig. 3. In the XRD pattern of Pd/C sample, the diffraction peaks at 2θ values of about 40.1°, 46.6°, 68.1°, 82.1° and 86.6° are associated with the (111), (200), (220), (311) and (222) planes, respectively, which consistent with a FCC (face centered cubic) crystal structure (JCPDS no. 05-0681) of Pd. In Pd-Co/G sample, the XRD pattern revealed the diffraction peaks for both Co (JCPDS no. 05-0727) and CoO (JCPDS no. 42-1300). Moreover, existence diffraction peaks at 2θ angles of 39.4°, 45.8°, 66.8°, 80.4° and 84.8° regarded to the (111), (200), (220), (311) and (222) reflection planes, respectively, which confirms a FCC crystal structure (JCPDS no. 87-0641) of Pd. Interestingly, compared to the pure Pd, each peak of Pd-Co shifts to a lower degree, indicating the presence of alloy composition in the Pd-Co catalyst [27].

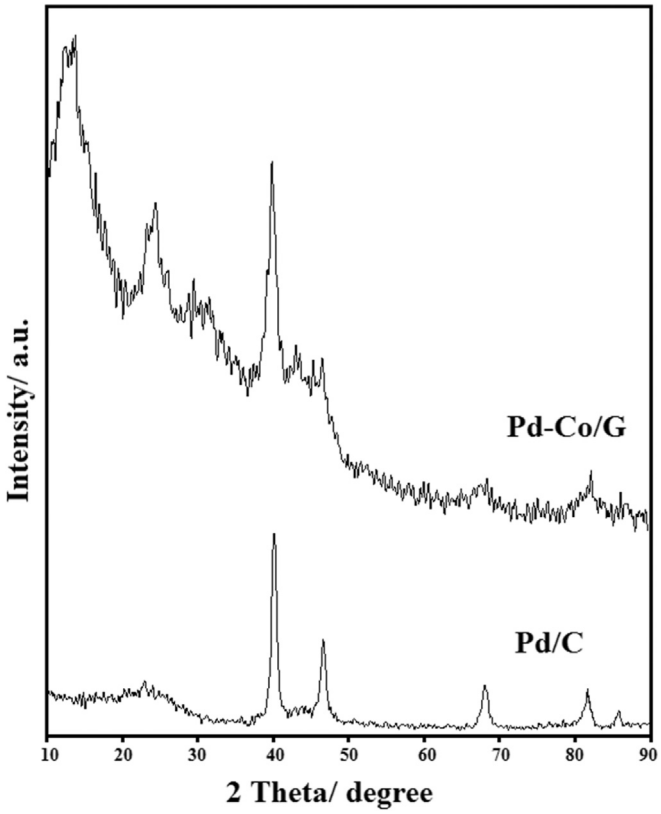

Fig. 3. X-ray diffraction (XRD) patterns of the Pd-Co/G and Pd/C catalysts.

The Energy Dispersive X-ray Spectroscopy (EDS) technique was used to determine the chemical composition of the as-produced Pd-Co/G electrocatalyst. Fig. 4 represents the EDS spectrum of the Pd-Co/G electrocatalyst after the galvanic replacement reaction of Co by Pd. The achieved results from the EDS spectrum in Fig. 4 are listed in Table (inset of Fig. 4). The EDS spectrum confirms the presence of Pd and Co in the Pd-Co/G electrocatalyst. On the basis of the elemental analysis of EDS spectrum, the elements mass percentages of Pd and Co in the fabricated electrocatalyst are equal to 7.92 and 1.05 wt%, respectively. The results also demonstrate that the galvanic replacement reaction between Pd and Co, simultaneously leads to the reduction of Pd. Also, according to the EDS spectrum and Table, Pd is the major element in the Pd-Co/G electrocatalyst.

Elemental EDS mapping was done to investigate the distribution of Co and Pd elements in the Pd-Co/G catalyst. Fig. 5(a) through 5(c) present element mapping of Co, Pd and Pd-Co mixed, respectively. It can be observed that, the Co and Pd nanoparticle are uniformly distributed, which may lead to the increase the electrocatalytic activity of Pd-Co/G catalyst.

3.3. Electrocatalytic performances

The electrochemical performances of the as-prepared Pd/C and Pd-Co/G electrocatalysts were recorded by cyclic voltammograms (CVs) in 0.5 M H_2SO_4 solution at a sweep rate of 50 mVs^{-1} at ambient condition. Fig. 6(a) represents the CV profiles of the Pd/C (red line) and Pd-Co/G (black line) electrocatalysts in 0.5 M H_2SO_4 solution and in the absence of formic acid with a sweep rate of 50 mVs^{-1} in the potential window −0.3 to +1.0 V *vs.* Ag/AgCl. In each CV profile, four major regions can be observed which are attributed to the hydrogen adsorption/desorption (I, IV), formation of PdO (II), and reduction of PdO (III) regions. According to the CV curves, the adsorption/desorption peak current densities of hydrogen are at the potential area −0.3 to 0.11 V. In addition, the desorption peak of hydrogen for the Pd-Co/G electrocatalyst is shifted clearly toward lower potentials, which means that the hydrogen adsorption strength on the Pd surface is weakened [2]. It can be seen that, oxidation of Pd surfaces is performed in the anodic sweep at potentials above 0.53 V. In the backward sweep, the reduction of the Pd oxides (PdO) can be obviously observed with a peak position at around 0.5 V. Obviously, the adsorption/desorption of hydrogen and formation and reduction of Pd (II) oxide peaks on the Pd-Co/G electrocatalyst are stronger in comparison to Pd/C electrocatalyst, which suggests that the Pd-Co/G electrocatalyst has

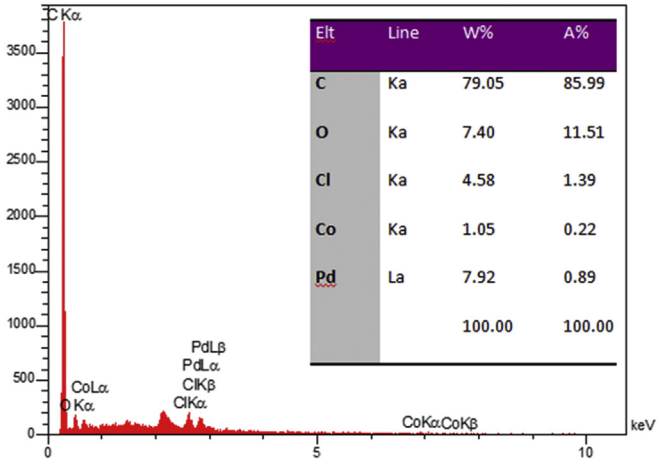

Elt	Line	W%	A%
C	Ka	79.05	85.99
O	Ka	7.40	11.51
Cl	Ka	4.58	1.39
Co	Ka	1.05	0.22
Pd	La	7.92	0.89
		100.00	100.00

Fig. 4. Elemental analysis of the Pd-Co/G catalyst.

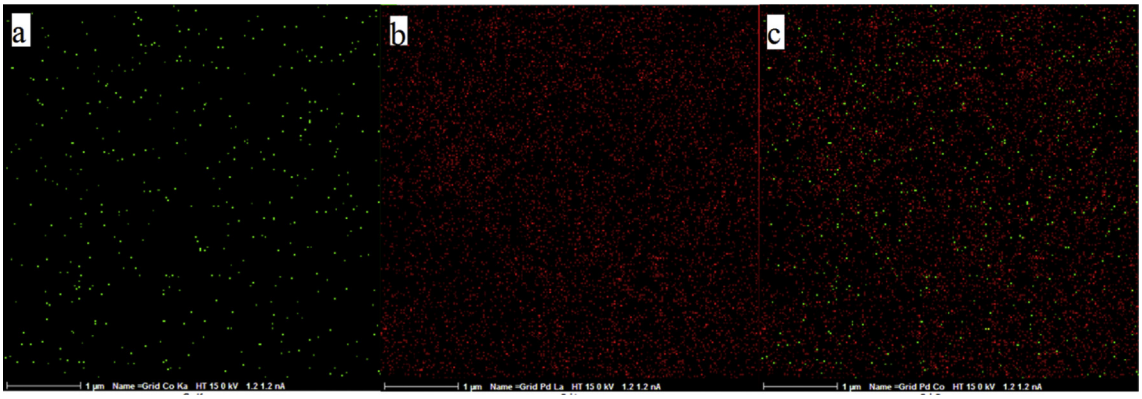

Fig. 5. Cobalt (a), palladium (b) and cobalt-palladium (c) elemental mapping.

a greater surface area and better electrocatalytic performance compared to the Pd/C. It has previously been demonstrated that the electrochemical active surface area (ECSA) of a catalyst is an important factor to evaluate the activity of an electrocatalyst [47]. Cyclic Voltammetry (CV) is a convenient and effective technique used to calculate the ECSA of a catalyst. The ECSA of a catalyst not only gives important information with relation to the number of electrochemically active sites per gram of the electrocatalyst, but also is a very important index to compare various electrocatalytic supports. In this work, to determine the ECSA for each catalyst, the surface oxide reduction approach was chosen due to the its low deviation [42]. Therefore, the values of ECSA for Pd-Co/G and Pd/C catalysts were achieved by utilizing the following eq. (10) [42]:

$$\mathrm{ECSA} = \frac{Q_R}{Q_{MR}} \tag{10}$$

where, Q_R is the columbic charge associated with the Pd (II) O reduction (in μC) while Q_{MR} is the charge needed for the reduction of Pd (II) O (424 μC cm^{-2}) monolayer. The values of ECSA for Pd/C and Pd-Co/G electrocatalysts were obtained to be 0.24 cm^2 and 0.82 cm^2, respectively. On the basis of ECSA values, it can be estimated that the electrocatalytic performance of Pd-Co/G electrocatalyst is superior compared to the Pd/C catalyst.

We compared the electrocatalytic activity of the as-produced Pd-Co/G electrocatalyst for the electrochemical oxidation of formic acid in 0.5 M H_2SO_4 with that of the Pd/C catalyst. The electrocatalytic performances of the as-fabricated Pd-Co/G and Pd/C electrocatalysts toward oxidation of formic acid were investigated by CVs measures in the mixture of a 0.5 M H_2SO_4 aqueous solution containing 0.5 M HCOOH at a sweep rate of 50 mVs^{-1} at ambient condition and the potential is swept from −0.3–1.0 V *vs*. Ag/AgCl (shown in Fig. 6(b)). It is generally agreed that the oxidation of formic acid proceeds on Pd surface mainly through the dehydrogenation pathway (direct pathway) without CO poisoning [48]. In each CV profile, in forward sweeps, the main oxidation peaks for Pd-Co/G and Pd/C were observed at 0.196 and 0.244 V, respectively, which is attributed to the oxidation of formic acid. Also, the small humps at around 0.5–0.7 V (Pd-Co/G) and 0.45–0.65 V (Pd/C) are associated with the oxidation of the Pd metal surfaces. In the backward sweeps, for each CV curve, there are two well-defined peaks; the peaks at about 0.5 to 0.35 V are attributed to the reduction of Pd (II) oxide, and at less positive potentials (0.216 V on Pd-Co/G and 0.243 V on Pd/C) the peaks are associated with the oxidation of formic acid on the newly reduced Pd metal surfaces. It can be observed that, the Pd-Co/G electrocatalyst not only delivered much superior current density (151.32 $mAcm^{-2}$) in comparison to the Pd/C catalyst (21.3 $mAcm^{-2}$), but also represented a more negative shift of the onset potential (−0.062 *vs* 0.037 V) in the forward sweep. The peak current density for the oxidation of formic acid on the Pd-Co/G electrocatalyst is 7.1 times superior compared to the Pd/C catalyst. Also, the oxidation peak potential of the formic acid oxidation reaction on the Pd-Co/G electrocatalyst (196 mV) is smaller in comparison to the Pd/C catalyst (244 mV), which suggests that the formic acid molecular is simply oxidized on the Pd-Co/G electrocatalyst. On the basic obtained results, the Pd-Co/G electrocatalyst demonstrates the better electrocatalytic activity

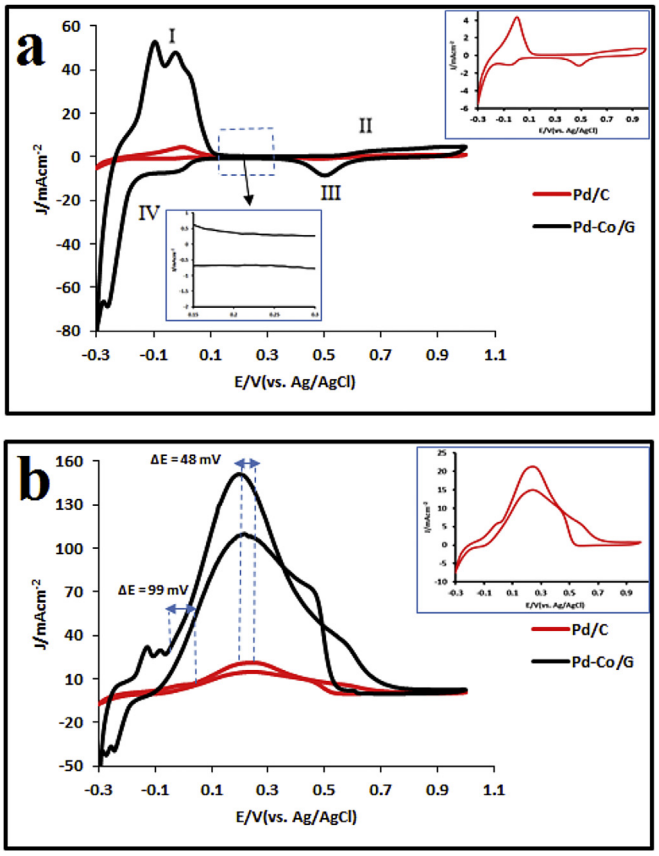

Fig. 6. Cyclic voltammograms of the as-prepared Pd-Co/G (black line) and Pd/C (red line) catalysts (a) in 0.5 M H_2SO_4 solution and (b) 0.5 M H_2SO_4 + 0.5 M HCOOH solution at scan rate of 50 mV s^{-1}. (For interpretation of the references to colour in this figure legend, the reader is referred to the Web version of this article.)

Table 1
Electrocatalytic activity results for the oxidation of formic acid on Pd-Co/G and Pd/C electrocatalysts.

Catalyst	Onset potential (mV)	Current density ($mAcm^{-2}$)	Peak potential (mV)	ECSA (cm^2)
Pd-Co/G	−62	151.32	+196	0.82
Pd/C	+37	21.3	+244	0.24

Table 2
Comparison of oxidation of formic acid at the surface of some modified electrodes containing Pd nanoparticles.

Electrode	Modifier	Electrolyte Concentration (M)	Formic acid Concentration (M)	Scan rate (mVs^{-1})	Current Density ($mAcm^{-2}$)	Ref.
GCE	Pd-Ag-100	0.1	0.5	100.0	3.9	[12]
GCE	Pd–P/C	0.5	0.5	50.0	18.4	[56]
GCE	Pd-Ag NWs[a]	0.1	0.5	20.0	0.9	[57]
GCE	Pd_1Co_1/CNF[b]	0.5	0.5	200.0	11.0	[13]
GCE	Pd NWs	0.1	0.1	50.0	2.5	[58]
GCE	Pd RBPs[c]	0.5	0.5	50.0	25.4	[59]
GCE	Cu/Pd	0.5	1.0	50.0	3.0	[42]
GCE	Pd NPs/G	0.1	0.1	50.0	0.95	[48]
GCE	Pd NDAs[d]	0.5	0.5	100.0	13.0	[60]
GCE	Pd-Co/G	0.5	0.5	50.0	151.32	this work

[a] PdAg nanowires.
[b] Pd_1Co_1/carbon nanofiber.
[c] Palladium right bipyramids.
[d] Pd nanodendrite assemblies.

for oxidation of formic acid compared to the Pd/C catalyst, which is primarily due to the synergistic effect (such as electronic effect, geometry effect, bifunctional mechanism, etc.), uniform distribution of catalyst, and presence of graphene nanosheets as catalyst support (see Table 1).

In Table 2, the current density for oxidation of formic acid in acidic condition with various electrodes containing Pd is shown. It can be observed that, the current density at the fabricated electrode (Pd-Co/G/GCE) is higher than other published works on modified electrodes for oxidation of formic acid. According to the data in

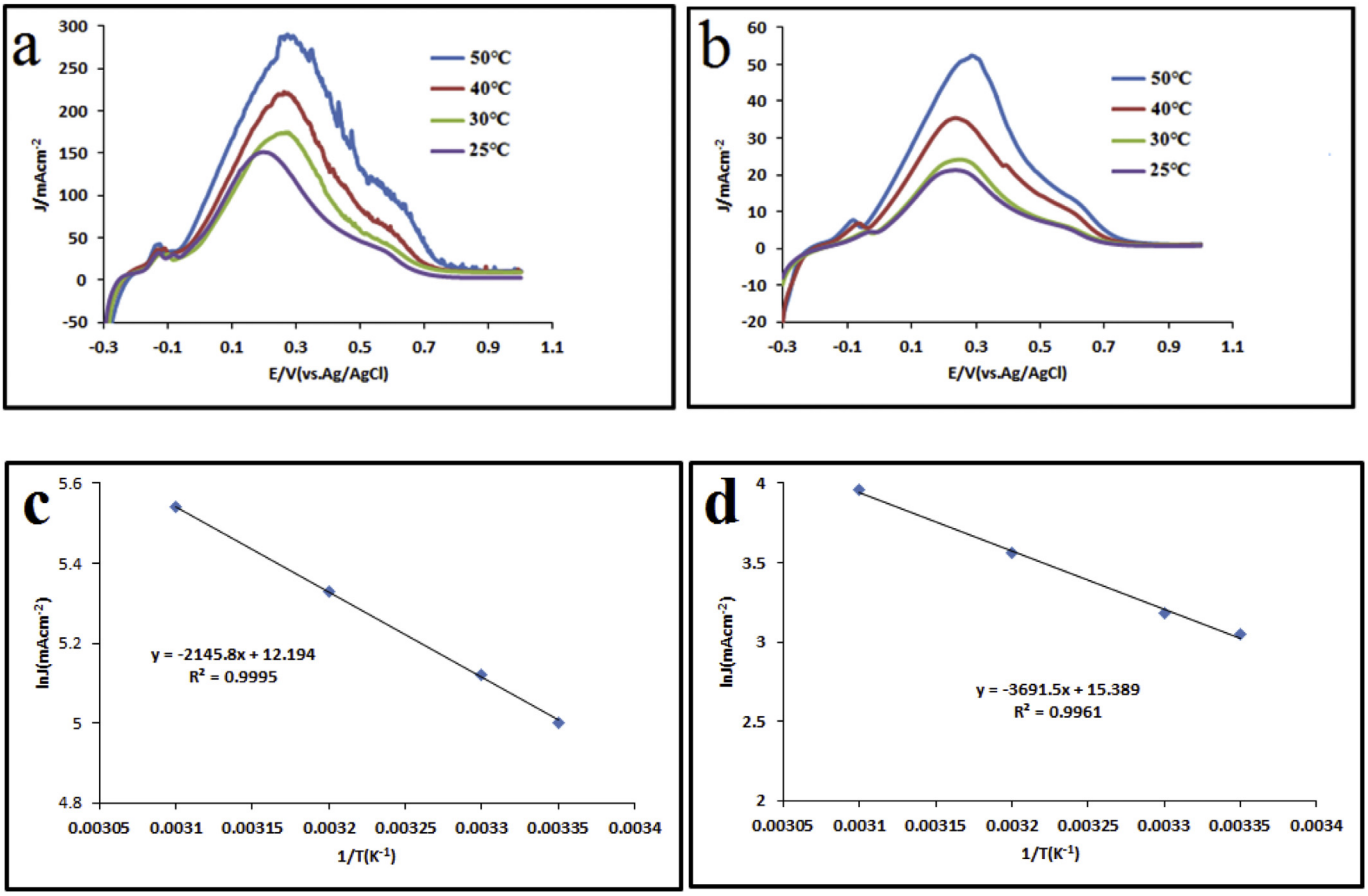

Fig. 7. LSV curves in the mixture of a 0.5 M H_2SO_4 and 0.5 M HCOOH solutions at different temperatures for Pd-Co/G (a) and Pd/C (b) Arrhenius plots for Pd-Co/G (c) and Pd/C (d) at +0.22 V (*vs.* Ag/AgCl) at scan rate of 50 mV s^{-1}.

Table 2, the proposed electrocatalyst seems to provide a favorable alternative for oxidation of formic acid.

To further illustrate the superior electrocatalytic behavior of the as-fabricated Pd-Co/G electrocatalyst, Linear Sweep Voltammetery (LSV) experiments were conducted at different temperatures (25, 30, 40, 50) on Pd-Co/G and Pd/C electrocatalyst (shown in Fig. 7 (a, b)). Fig. 7 (c, d) exhibit the relationship of the ln I versus T^{-1} at E = 0.22 V. The apparent activation energy (Ea) for both electrocatalysts has been obtained by plotting ln I as a function of T^{-1} at a given potential using the Arrhenius eq. (11) [49]:

$$I = Ae^{-E_a/RT} \quad (11)$$

where, I is the current density at a given potential, R, T and Ea are the gas constant, temperature (per K) and apparent activation energy at a given potential, respectively. By linear fit of ln I versus T^{-1}, Ea can be determined for Pd-Co/G and Pd/C electrocatalysts at 17.8 and 30.7 kJmol^{-1}, respectively. Clearly, the value of apparent activation energy for Pd-Co/G electrocatalyst is smaller compared to the Pd/C catalyst; this is indicative of higher intrinsic activity and faster charge transfer process for Pd-Co/G catalyst.

The effect of potential scan rate on the oxidation of formic acid on the Pd-Co/G was investigated by using CV at various scan rates in the mixture of a 0.5 M HCOOH and 0.5 M H_2SO_4 solution at ambient condition (shown in Fig. 8(a)). The results demonstrated that the oxidation peak current density of formic acid clearly increased with the increase of scan rate. Moreover, Fig. 8(b) exhibits a good linear relationship between the oxidation peak current and the square root of scan rates ($\upsilon^{1/2}$). Based on the observed linear relationship, it is suggested that the oxidation of formic acid may be controlled by a diffusion process [50,51].

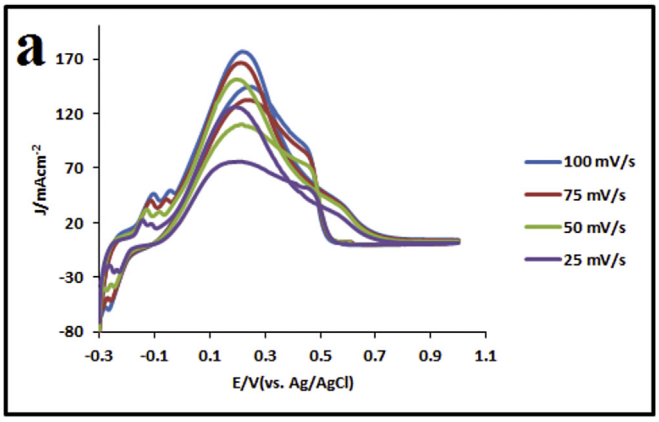

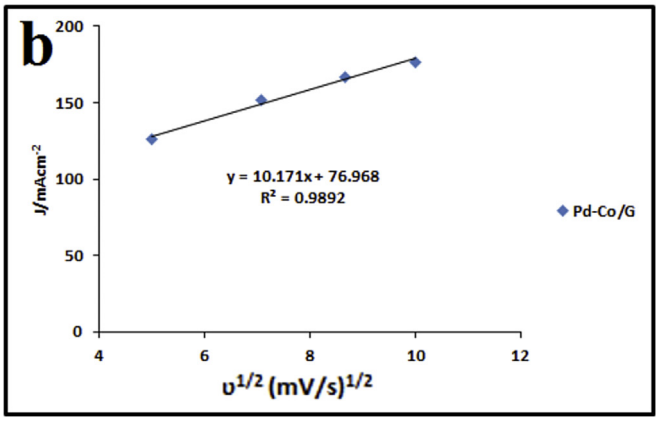

Fig. 8. (a) CV curves of the formic acid oxidation on the Pd-Co/G at different scan rates in the 0.5 M H_2SO_4 + 0.5 M HCOOH solution, and (b) plot of forward peak current density *vs.* the square root of the scan rate.

It is well-known that, the stability of an electrocatalyst is an important index for the commercial application of a catalyst. However, redox processes on the surface of electrocatalysts often lead to the deactivation of electrocatalytic activity. To evaluate the electrocatalytic activity and stability of the as-produced Pd/C and Pd-Co/G electrocatalysts, chronoamperometry (CA) was conducted at a potential of 0.25 V *vs.* Ag/AgCl for 1000s in the mixture of a 0.5 M H_2SO_4 + 0.5 M HCOOH solution at a sweep rate of 50 mVs^{-1} in ambient condition (shown in Fig. 9). Fig. 9 represents the corresponding current–time curves of the as-produced Pd-Co/G and Pd/C electrocatalysts. As shown, in initial steps of CA measures, the Pd/C and Pd-Co/G electrocatalysts illustrated a high current density, which is primarily because of two reasons: (1) the double layer charging process and (2) the existence of large available active sites on both electrocatalysts surface. A dramatic decay of the current density with time occurred in early step of CA experiments of Pd-Co/G and Pd/C electrocatalysts due to the agglomeration of intermediate species on the active sites of Pd-Co/G and Pd/C which leads to the poisoning of electrocatalyst surfaces [18–37]. After the quick decay in current densities, activities were stabilized at 51.7 mAcm^{-2} on Pd-Co/G and 3.3 mAcm^{-2} on Pd/C, respectively. These results exhibit that Pd-Co/G electrocatalyst has superior stability and electrocatalytic performance compared to the Pd/C electrocatalyst.

Electrochemical Impedance Spectroscopy (EIS) is used to investigate the capacitance of fuel cell catalyst layers. It has been established that limiting capacitance correlates with active area [52]. Impedance measurements were carried out to further study the electrochemical behaviors of Pd-Co/G and Pd/C electrocatalysts. Fig. 10 represents the Nyquist plots of the as-prepared Pd-Co/G and Pd/C electrocatalysts. The Nyquist plots illustrate that the charge transfer process occurs on the surface of both electrocatalysts. In general, the increase in the diameter of the semicircle leads to an increase in the charge transfer resistance (R_{CT}) and a lower R_{CT} value demonstrates a faster rate of charge transfer process [53,54]. The values of R_{CT} are approximately 59.6 Ω and 535 Ω for Pd-Co/G and Pd/C electrocatalysts, respectively. To measure the electrocatalytic performance, the standard exchange current density (i_0) is often used which can be determined according to the following relationship (12) [55].

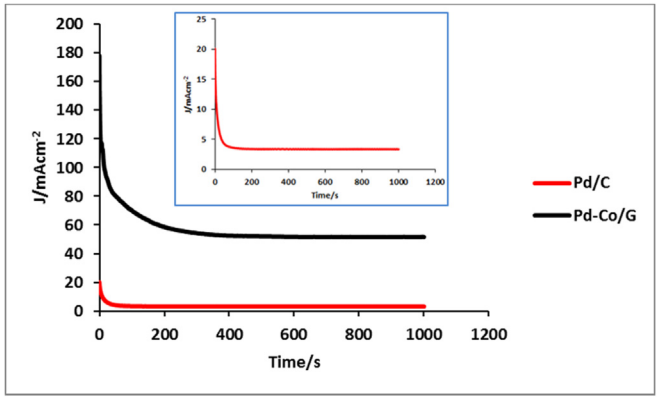

Fig. 9. Chronoamperometry curves of the Pd-Co/G (black curve) and Pd/C (red curve) in 0.5 M H_2SO_4 + 0.5 M HCOOH solution at potential of 0.25 V (*vs.* Ag/AgCl). (For interpretation of the references to colour in this figure legend, the reader is referred to the Web version of this article.)

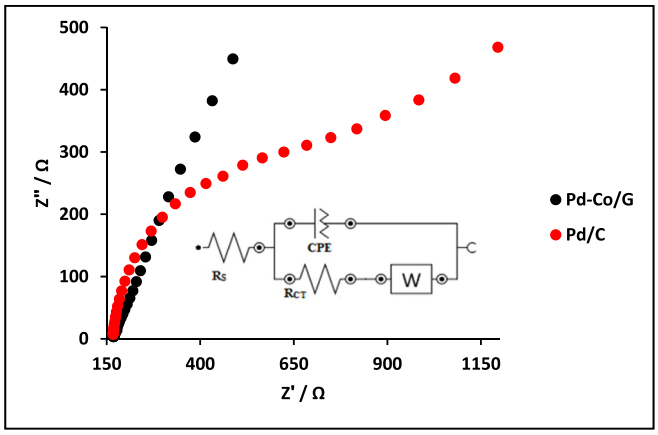

Fig. 10. The Nyquist plots recorded at potential of 0 V for the Pd-Co/G and Pd/C in the solution of 5 mM $[Fe(CN)_6]^{3-/4-}$ prepared in 0.1 M KCl.

$$i_0 = RT/nFR_{CT} \quad (12)$$

where, n is the number of electrons involved in the charge transfer reaction (n = 1), while T, F, R, and R_{CT} are the absolute temperature per Kelvin, Faradic constant, gas constant, and charge transfer resistance in Ω, respectively. A greater i_0 represents superior catalytic activity. The values of i_0 for Pd/C and Pd-Co/G catalysts were estimated 0.48 × 10^{-4} and 4.3 × 10^{-4} mA, respectively. These values were calculated according to the Nyquist plots in Fig. 10 and relationship (12). This result demonstrates that the electron-transfer kinetics is largely facilitated on the Pd-Co/G electrocatalyst which is in excellent agreement with the electrochemical results.

4. Conclusion

In summary, we have demonstrated a simple, very fast, inexpensive, and environmentally friendly approach to fabricate Pd-Co/G electrocatalyst using two steps: (1) electrochemical reduction of cobalt (II) formate in HCl (5 wt%) aqueous solution and (2) the galvanic replacement Co by Pd^{2+} ions. The peak current density of formic acid oxidation reaction on Pd-Co/G was very high (151.32 mA cm^{-2}). Moreover, its stability was remarkably promoted. The Pd-Co/G electrocatalyst prepared in this study illustrates extraordinary electrocatalytic activity and durability toward formic acid oxidation. This can, be ascribed to the synergistic effect (e.g. electronic effect and bifunctional mechanism, etc.). Apart from the synergistic effect, the uniform distribution of catalyst on graphene nanosheets and the presence of graphene nanosheets as catalyst support increased the electrocatalytic activity of the Pd-Co/G electrocatalyst. The novel Pd-Co/G electrocatalyst shows large electrochemically active surface area (ECSA), excellent catalytic activity, superior level of stability and lower charge transfer resistance (R_{CT}) compared to the Pd/C toward oxidation of formic acid.

References

[1] F. Zhu, M. Wang, Y. He, G. Ma, Z. Zhang, X. Wang, A comparative study of elemental additives (Ni, Co and Ag) on electrocatalytic activity improvement of PdSn-based catalysts for ethanol and formic acid electro-oxidation, Electrochim. Acta 148 (2014) 291–301.
[2] D.-N. Li, A.-J. Wang, J. Wei, Q.-L. Zhan, J.-J. Feng, Facile synthesis of flower-like Au@AuPd nanocrystals with highly electrocatalytic activity for formic acid oxidation and hydrogen evolution reactions, Int. J. Hydrog. Energy 42 (2017) 19894–19902.
[3] K. Wang, B. Wang, J. Chang, L. Feng, Wei Xing, Formic acid electrooxidation catalyzed by Pd/S_mO_x-C hybrid catalyst in fuel cells, Electrochim. Acta 150 (2014) 329–336.
[4] S.M. Baik, J. Kim, J. Han, Y. Kwon, Performance improvement in direct formic acid fuel cells (DFAFCs) using metal catalyst prepared by dual mode spraying, Int. J. Hydrog. Energy 36 (2011) 12583–12590.
[5] Y. Zhua, Z. Khana, R.I. Masel, The behavior of palladium catalysts in direct formic acid fuel cells, J. Power Sources 139 (2005) 15–20.
[6] A. Ciftci, D.A.J. Michel Ligthart, P. Pastorino, E.J.M. Hensen, Nanostructured ceria supported Pt and Au catalysts for the reactions of ethanol and formic acid, Appl. Catal. B Environ. 130–131 (2013) 325–335.
[7] Ch. V. Rao, C.R. Cabrera, Y. Ishikawa, Graphene-supported Pt_Au alloy nanoparticles: a highly efficient anode for direct formic acid fuel cells, J. Phys. Chem. C 115 (2011) 21963–21970.
[8] Sh. Zhang, Y. Shao, G. Yin, Y. Lin, Electrostatic self-assembly of a Pt-around-Au nanocomposite with high activity towards formic acid oxidation, Angew. Chem. Int. Ed. 49 (2010) 2211–2214.
[9] Y. Jiang, Y. Lu, D. Han, Q. Zhang, L. Niu, Hollow Ag@Pd core-shell nanotubes as highly active catalysts for the electro-oxidation of formic acid, Nanotechnology 23 (2012) 105609–105618.
[10] M. Shao, K. Sasaki, R.R. Adzic, Pd-Fe nanoparticles as electrocatalysts for oxygen reduction, J. Am. Chem. Soc. 128 (2006) 3526–3527.
[11] Qiang Wang, Yuxiang Liao, Heyou Zhang, Jun Li, Wei Zhao, Shengli Chen, One-pot synthesis of carbon-supported monodisperse palladium nanoparticles as excellent electrocatalyst for ethanol and formic acid oxidation, J. Power Sources 292 (2015) 72–77.
[12] Y. Lu, W. Chen, Nanoneedle-covered Pd-Ag nanotubes: high electrocatalytic activity for formic acid oxidation, J. Phys. Chem. C 114 (2010) 21190–21200.
[13] D. Liu, Q. Guo, H. Hou, O. Niwa, T. You, Pd_xCo_y nanoparticle/carbon nanofiber composites with enhanced electrocatalytic properties, ACS Catal. 4 (2014) 1825–1829.
[14] R. Jana, U. Subbarao, S.C. Peter, Ultrafast synthesis of flower-like ordered Pd3Pb nanocrystals with superior electrocatalytic activities towards oxidation of formic acid and ethanol, J. Power Sources 301 (2016) 160–169.
[15] M. Sh. Ahmed, D. Park, S. Jeon, Ultrasmall $Pd_mMn_{1-m}O_x$ binary alloyed nanoparticles on graphene catalysts for ethanol oxidation in alkaline media, J. Power Sources 308 (2016) 180–188.
[16] L. Lua, L. Shena, Y. Shia, T. Chenb, G. Jiangb, C. Geb, Y. Tanga, Y. Chena, T. Lu, New insights into enhanced electrocatalytic performance of carbon supported Pd-Cu catalyst for formic acid oxidation, Electrochim. Acta 85 (2012) 187–194.
[17] R.D. Morgan, A. Salehi-khojin, R.I. Masel, Superior formic acid oxidation using carbon nanotube-supported palladium catalysts, J. Phys. Chem. C 115 (2011) 19413–19418.
[18] I.A. Rutkowska, D. Marks, Ch. Perruchot, M. Jouini, P.J. Kulesz, Admixing palladium nanoparticles with tungsten oxide nanorods toward more efficient electrocatalytic oxidation of formic acid, Colloids Surf. A: Physicochem. Eng. Aspects 439 (2013) 200–206.
[19] Ch. Peng, Y. Hu, M. Liu, Y. Zheng, Hollow raspberry-like PdAg alloy nanospheres: high electrocatalytic activity for ethanol oxidation in alkaline media, J. Power Sources 278 (2015) 69–75.
[20] Y.G. Jo, S.M. Kim, J.-W. Kim, S.Y. Lee, Composition-tuned porous Pd-Ag bimetallic dendrites for the enhancement of ethanol oxidation reactions, J. Alloys Compd. 688 (2016) 447–453.
[21] R. Li, Z. Wei, T. Huang, A. Yu, Ultrasonic-assisted synthesis of Pd-Ni alloy catalysts supported on multi-walled carbon nanotubes for formic acid electrooxidation, Electrochim. Acta 56 (2011) 6860–6865.
[22] Zh. Liu, X. Zhang, S.W. Tay, Nanostructured PdRu/C catalysts for formic acid oxidation, J. Solid State Electrochem. 16 (2012) 545–550.
[23] T. Maiyalagan, Xin Wanga, A. Manthiram, Highly active Pd and Pd–Au nanoparticles supported on functionalized graphene nanoplatelets for enhanced formic acid oxidation, RSC Adv. 4 (2014) 4028.
[24] H. Xu, B. Yan, K. Zhang, J. Wang, Sh. Li, C. Wang, Y. Shiraishi, Y. Du, P. Yang, Facile fabrication of novel PdRu nanoflowers as highly active catalysts for the electrooxidation of methanol, J. Colloid Interface Sci. 505 (2017) 1–8.
[25] H. Xu, K. Zhang, B. Yan, J. Wang, C. Wang, Sh. Li, Z. Gu, Y. Du, Ultra-uniform PdBi nanodots with high activity towards formic acid, J. Power Sources 356 (2017) 27–35.
[26] H. Xu, B. Yan, K. Zhang, J. Wang, Sh. Li, C. Wang, Y. Shiraishi, Y. Du, P. Yang, Ultrasonic-assisted synthesis of N-doped graphene-supported binary PdAu nanoflowers for enhanced electro-oxidation of ethylene glycol and glycerol, Electrochim. Acta 245 (2017) 227–236.
[27] H. Xu, B. Yan, K. Zhang, J. Wang, Sh. Li, C. Wang, Z. Xiong, Y. Shiraishi, Y. Du, Self-supported worm-like PdAg nanoflowers as efficient electrocatalysts towards ethylene glycol oxidation Highly, ChemElectroChem 4 (2017) 2527–2534.
[28] Y. Huang, X. Zhou, M. Yin, Ch. Liu, W. Xing, Novel PdAu@Au/C core-shell catalyst: superior activity and selectivity in formic acid decomposition for hydrogen generation, Chem. Mater. 22 (2010) 5122–5128.
[29] X. Wang, Y. Xia, Electrocatalytic performance of PdCo-C catalyst for formic acid oxidation, Electrochem. Commun. 10 (2008) 1644–1646.
[30] P. Mukherjee, J. Bagchi, S. Dutta, S.K. Bhattacharya, The nickel supported platinum catalyst for anodic oxidation of ethanol in alkaline Medium, Appl. Catal. A Gen. 506 (2015) 220–227.
[31] R.C. Sekol, X. Li, P. Cohen, G. Doubek, M. Carmo, A.D. Taylor, Silver palladium core–shell electrocatalyst supported on MWNTs for ORR in alkaline media, Appl. Catal. B Environ. 138–139 (2013) 285–293.

[32] F. Munoz, Ch. Hua, T. Kwong, L. Tran, T.Q. Nguyen, J.L. Haan, Palladium–copper electrocatalyst for the promotion of the electrochemical oxidation of polyalcohol fuels in the alkaline direct alcohol fuel cell, Appl. Catal. B Environ. 174 (2015) 323–328.
[33] D. Morales-Acostaa, J. Ledesma-Garciab, L.A. Godineza, H.G. RodrÍguez, L. Álvarez-Contrerasc, L.G. Arriagaa, Development of Pd and Pd–Co catalysts supported on multi-walled carbon nanotubes for formic acid oxidation, J. Power Sources 195 (2010) 461–465.
[34] L. Zhang, L. Wan, Y. Ma, Y. Chen, Y. Zhou, Y. Tang, T. Lu, Crystalline palladium–cobalt alloy nano assemblies with enhanced activity and stability for the formic acid oxidation reaction, Appl. Catal. B Environ. 138–139 (2013) 229–235.
[35] R. Wang, Sh. Liao, Sh. Ji, High performance Pd-based catalysts for oxidation of formic acid, J. Power Sources 180 (2008) 205–208.
[36] L.Y. Zhang, Zh. L. Zhao, W. Yuana, Ch. M. Li, Facile one-pot surfactant-free synthesis of uniform Pd6Co nanocrystals on 3D graphene as an efficient electrocatalyst toward formic acid oxidation, Nanoscale 8 (2016) 1905–1909.
[37] V. Mazumder, M. Chi, M.N. Mankin, Y. Liu, Ö. Metin, D. Sun, K.L. More, Sh. Sun, A facile synthesis of MPd (M = Co, Cu) nanoparticles and their catalysis for formic acid oxidation, Nano Lett. 12 (2012) 1102–1106.
[38] M. Yin, Q. Li, J.O. Jensen, Y. Huang, L.N. Cleemann, N.J. Bjerrum, W. Xing, Tungsten carbide promoted Pd and Pd-Co electrocatalysts for formic acid Electrooxidation, J. Power Sources 219 (2012) 106–111.
[39] D. Morales-Acostaa, M.D. Morales-Acostab, L.A. Godineza, L. Alvarez-Contrerasc, S.M. Duron-Torresd, J. Ledesma-Garciaa, L.G. Arriagaa, PdCo supported on multi-walled carbon nanotubes as an anode catalyst in a microfluidic formic acid fuel cell, J. Power Sources 196 (2011) 9270–9275.
[40] C. Xu, Y. Liu, H. Zhang, H. Geng, A nanoporous PdCo alloy as a highly active electrocatalyst for the oxygen-reduction reaction and formic acid electrooxidation, Chem. Asian J. 8 (2013) 2721–2728.
[41] J.H. Seo, I. Jo, A.L. Moore, L. Lindsay, Z.H. Aitken, M.T. Pettes, X. Li, Zh. Yao, R. Huang, D. Broido, N. Mingo, R.S. Ruoff, L. Shi, Two-dimensional phonon transport in supported graphene, Science 328 (9) (2010) 213–216.
[42] R. Ojani, Z. Abkar, E. Hasheminejad, J. Raoof, Rapid fabrication of Cu/Pd nano/micro-particles porous-structured catalyst using hydrogen bubbles dynamic template and their enhanced catalytic performance for formic acid electrooxidation, Int. J. Hydrog. Energy 39 (2014) 7788–7797.
[43] W. Hummersjr, R. Offeman, Preparation of graphitic oxide, J. Am. Chem. Soc. 80 (6) (1958), 1339–1339.
[44] J. Luo, S. Jiang, H. Zhang, J. Jiang, X. Liu, A novel non-enzymatic glucose sensor based on Cu nanoparticle modified graphene sheets electrode, Anal. Chim. Acta 709 (2012) 47–53.
[45] W. Li, X. Zhao, A. Manthiram, Room-temperature synthesis of Pd/C cathode catalysts with superior performance for direct methanol fuel cells, J. Mater. Chem. A 2 (2014) 3468–3476.
[46] H. Rostami, A.A. Rostami, A. Omrani, Investigation on ethanol electrooxidation via electrodeposited Pd-Co nanostructures supported on graphene oxide, Int. J. Hydrog. Energy 40 (2015) 10596–10604.
[47] Y. Li, W. Gao, L. Ci, Ch. Wang, P.M. Ajayan, Catalytic performance of Pt nanoparticles on reduced graphene oxide for methanol electro-oxidation, Carbon 48 (2010) 1124–1130.
[48] T. Jin, Sh. Guo, J. Zuo, Sh. Sun, Synthesis and assembly of Pd nanoparticles on graphene for enhanced electrooxidation of formic acid, Nanoscale 5 (2013) 160–163.
[49] Y. Zhao, S. Nie, H. Wang, J. Tian, Zh. Ning, X. Li, Direct synthesis of palladium nanoparticles on Mn3O4 modified multi-walled carbon nanotubes: a highly active catalyst for methanol electro-oxidation in alkaline media, J. Power Sources 218 (2012) 320–330.
[50] X. Wang, W. Wang, Zh. Qi, Ch. Zhao, H. Ji, Zh. Zhang, Electrochemical catalytic activities of nanoporous palladium rods for methanol electro-oxidation, J. Power Sources 195 (2010) 6740–6747.
[51] W. Yea, Y. Chen, Y. Zh, J. Fub, W. Wub, D. Gaoa, F. Zhouc, Ch. Wang, D. Xue, Enhancing the catalytic activity of flowerlike Pt nanocrystals using polydopamine functionalized graphene supports for methanol electrooxidation, Electrochim. Acta 142 (2014) 18–24.
[52] E.B. Easton, P.G. Pickup, An electrochemical impedance spectroscopy study of fuel cell electrodes, Electrochim. Acta 50 (2005) 2469–2474.
[53] H. Chen, Y. Huang, D. Tang, T. Zhang, Y. Wang, Ethanol oxidation on Pd/C promoted with CaSiO3 in alkaline medium, Electrochim. Acta 158 (2015) 18–23.
[54] F. Yang, Y. Zhang, P. Liu, Y. Cui, X. Ge, Q. Jing, Pd-Cu alloy with hierarchical network structure as enhanced electrocatalysts for formic acid oxidation, Int. J. Hydrog. Energy 41 (2016) 6773–6780.
[55] A. Shafaei Douk, H. Saravani, M. Noroozifar, Novel fabrication of PdCu nanostructures decorated on graphene as excellent electrocatalyst toward ethanol oxidation, Int. J. Hydrog. Energy 42 (2017) 15149–15159.
[56] G. Yang, Y. Chen, Y. Zhou, Y. Tang, T. Lu, Preparation of carbon supported Pd–P catalyst with high content of element phosphorus and its electrocatalytic performance for formic acid oxidation, Electrochem. Commun. 12 (2010) 492–495.
[57] Y. Lu, W. Chen, PdAg alloy nanowires: facile one-step synthesis and high electrocatalytic activity for formic acid oxidation, ACS Catal. 2 (2012) 84–90.
[58] Y. Wang, S. Choi, X. Zhao, Sh. Xie, H. Peng, M. Chi, Ch. Zh. Huang, Y. Xia, Polyol synthesis of ultrathin Pd nanowires via attachment-based growth and their enhanced activity towards formic acid oxidation, Adv. Funct. Mater. 24 (18) (2014) 131–139.
[59] X. Xia, S. Ch, J.A. Herron, N. Lu, J. Scaranto, H. Peng, J. Wang, M. Mavrikakis, M.J. Kim, Y. Xia, Facile synthesis of palladium right bipyramids and their use as seeds for overgrowth and as catalysts for formic acid oxidation, J. Am. Chem. Soc. 135 (42) (2013) 15706–15709.
[60] L. Zhang, Q. Sui, T. Tang, Y. Chen, Y. Zhou, Y. Tang, T. Lu, Surfactant-free palladium nanodendrite assemblies with enhanced electrocatalytic performance for formic acid oxidation, Electrochem. Commun. 32 (2013) 43–46.